Hindawi
Journal of Nanomaterials
Volume 2022, Article ID 1111657, 15 pages
https://doi.org/10.1155/2022/1111657

Research Article

Effect of Nanoparticles on Wire Surface Coating Using Viscoelastic Third-Grade Fluid as a Coating Polymer inside Permeable Covering Die with Variable Viscosity and Magnetic Field

Zeeshan Khan,[1] Ilyas Khan,[2] N. Ameer Ahammad,[3] D. Baba Basha,[4] and Mulugeta Andualem[5]

[1]*Department of Mathematics and Statistics, Bacha Khan University Charsadda, KP, Pakistan*
[2]*Department of Mathematics, College of Science Al-Zulfi, Majmaah University, Al-Majmaah 11952, Saudi Arabia*
[3]*Department of Mathematics, Faculty of Science, University of Tabuk, P.O.Box.741, Tabuk 71491, Saudi Arabia*
[4]*Department of Physics, College of Computer and Information Sciences, Majmaah University, Al-Majmaah, 11952, Saudi Arabia*
[5]*Department of Mathematics, Bonga University, Bonga, Ethiopia*

Correspondence should be addressed to Ilyas Khan; i.said@mu.edu.sa and Mulugeta Andualem; mulugetaandualem4@gmail.com

Received 16 September 2021; Accepted 13 April 2022; Published 6 May 2022

Academic Editor: Vidyadhar Singh

Goal. The parameters of coated wire products are determined by momentum and heat transmission inside dies. As a consequence, it is essential to understand the polymerization movement, heat mass transmission, and wall stress concentration. The wire covering technique necessitates a boost in thermal efficiency. As a result, the goal of this study is to see how nanomaterials affect the heat and mass transfer mechanisms of third-grade liquid in wire coating analysis. The Buongiorno model is adopted for nanofluids. *Methodology/approach*. Continuity, momentum, energy, and nanoparticle volume fraction concentration is used to establish the governing equations. For highly nonlinear, the numerical methodology bvph2 technique is applied to yield numerical solutions. The impacts of the input parameters on motion, temperature, and volume fraction are examined using pictorial representations. Moreover, using the ND-solve, the numerical results are validated analytically. *Findings*. In Reynolds Modeling, the stress on the entire wire surface integrated shear forces at the surface dominate Vogel's model, according to the analytical conclusions of this inquiry. It is observed that the nanomaterials appear to have a favorable impact on wire force throughout the entire surface and shear forces at the surface. The polymer velocity can be increased using a non-Newtonian parameter. The temperature profile is increased in the first half of the segment with larger values of random motion and nonlinear thermal while decreases in the later part. In addition, the Brownian motion component raises the concentration profile, but the thermophoresis factor decreases it. *Practical implications*. This research could aid in the advancement of wire coating technologies. *Originality/value*. For the first time, Brownian motion with generation/absorption slippage processes is used to investigate the importance of nanoparticles in wire coating assessment. Two different models are utilized for time-dependent viscosity: Reynolds and Vogel models.

1. Introduction

Studying and analysing non-Newtonian fluids is of significant curiosity together with theoretical and applied viewpoint [1, 2]. Fluid dynamics and material science awareness related to non-Newtonian fluid motion may have major ramifications in a variety of fields, including polymer preparation, protecting and lacquer, ink-jet printing, aerodynamics, homodynamics, turbulent shear stream, slurry and ingredient suspensions, and blood serum. As a result, there has been a lot of focus on these movements, and the bibliography has a lot of work on statistical, theoretical, and

algebraic solutions on the subject [3, 4]. Furthermore, the mobility of such fluids poses significant problems to professionals from a variety of study domains, including computational models, economics, mathematics, and physics. In fact, when contrasted to Newtonian fluids, the equations postulated and produced for non-Newtonian concepts are far more difficult. The modelled equation of non-Newtonian fluids is highly nonlinear, making exact solutions extremely difficult to acquire [5–8]. It is also difficult to obtain extremely precise estimates for viscous liquids regarding the nonlinear and utterly irrelevant nature of the aggregation concept [5–8]. Many scholars have devised analytical and numerical techniques to solve these nonlinear problems for this goal.

Wire coating (an extrusion method) is usually applied in the polymerization sector designed for insulating material and protection against mechanical injury. An uncovered warmed wire is immersed and pulled into the melting resin in this technique. Extruding the heated polymer across a rolling wire is also used for this operation. A conventional wire coating machine has five separate components: a payoff device, a wire preheating instrument, an extrusion, a chilling system, and a pull device. Tubing-type die and pressurized die are the most popular dies used for wire treatments. The latter, which resembles an annulus, is typically utilized wire coating.

As a result, flows through such dies resemble flows across an annular region established by a pair of concentric cylinders. The inner cylinder travels axially, while the exterior cylinder remains stationary. Many researchers [9–14] employed power-law and Newtonian frameworks to describe the rheological behavior of the emulsion polymerization flow in early studies. The wire sealant examination employing a pressure form die is presented in [15, 16]. Following then, [17–20] provided more scientific work on the subject. Mitsoulis [21] also provides a comprehensive overview of heat transmission and melted movement in wire veneer. Akter and Hashmi [22] investigated wire coating using a pressurized die. Later, using a cylindrical unit, Akter and Hashmi investigated melting flow throughout the wire coating processes [23, 24].

Wire shell is an advanced production method for insulating and protecting wires from the environment. The immersion process, coaxial method, and electromagnetic deposit process are the three categories of wire covering. The dipping progression creates a significantly stronger relationship between the continuums, but it is somewhat sluggish in equated to the other two methods. Han and Rao [25] evaluated the issues associated with coating extrusion using a pressurized type die. The extrusion procedure is made up of three parts: the feeder entity, the chamber, then the cranium through a die. Kozan and Cirak [26] reported on the extensive deliberations of these three unique parts. In particular, Sajid et al. [27] used the HAM method to explain and handle the wire coating operations of Oldroyd 8-constant fluid. Likewise, Shah et al. [28] used the perturbation methodology to examine the wiring layer of viscoelastic third-grade fluid and presented their findings in [28].

The Phan-Thein-Tanner (PTT) model, a third-grade non-Newtonian molten, is currently the utmost widely adopted wire coating prototype. Binding et al. [29] investigated the rising wire-coating procedure for viscoelastic fluids in a viscoelastic constitutive model. It also studied the flaws of the actual modeling technique. The wire coating study based on the pipe die was supplied by Multu et al. [30]. Kasajima and Ito [31] investigated the wire coating technique of polymer produced until then. They also focused on how heat transfer affects cooling coatings. Baag and Mishra [32] explored wire coating using the temperature linearly varying at the boundary. Similarly, two-layer coating was investigated by many researchers [33–37].

For recent times, the issue of heat transfer improvement has gotten a lot of attention. Thermoelectric scientists have proposed that nanotube metallic or nonmetallic materials be added to conventional fluids to increase thermal properties since nanoparticles have better thermal conductivity than the base liquid. Nanofluid is the resultant mixture that has improved physicochemical properties. Aziz [38] developed first time the terminology of nanofluid in 1995. Furthermore, a special type of nanofluid known as hybrid nanofluid is studied to boost thermal efficiency. Some other related studies can be found in [39–53].

This investigation was aimed at studying the effects of nanomaterials proceeding the MHD third-grade fluid in a pressurized sort die during the wire surface layer using Brownian motion in addition to heat conduction.

Numerical solutions have been achieved via Runge-Kutta 4^{th} order scheme [48–52]. Reynolds, as well as Vogel's models, compensates for variable viscosity as well. Such an endeavor has still not been constructed to the aim to contribute. Before being attempted analytically, the relevant resulting equations are made dimensionless by suitable transformation factors. The effect of various parameters accessing the problem is investigated in two situations: (1) the Reynolds model and (2) Vogel's model.

2. Modeling of the Problem

Figure 1 depicts the flow problem's geometry, wherein the wire is pulled within a cylinder fed with third-grade nanofluid as a coating substance. The electrical field is presented towards the fluid in a normal direction. Because of the low Reynolds number, the reto magnetic field is expected to be insignificant, which really is adequate in the experiment. The location of the continuum is believed to be concentrically situated. $(Rw, \theta w, \phi w)$ and $(Rd, \theta d, \phi d)$ are the radius, temperature, and volume fraction of the wire as well as die, compatibly.

Uw is also the speed of the said wire as it is inserted along the central path of the die. The emulsion polymerization flow should be axisymmetric, continuous, and homogeneous. Han and Rao [12] evaluate the velocity, additional stress tensor, heating rate, and volume fraction of nanomaterials:

$$\vec{w} = [0, 0, \mathrm{w}(r)], S = S(r), T = T(r). \quad (1)$$

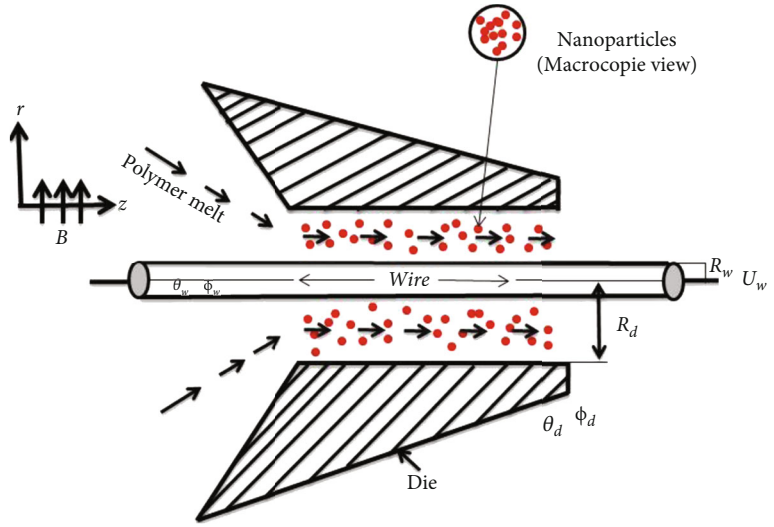

Figure 1: Two-phase coating geometry.

Substance to constraints

$$w = Uw, \theta = \theta w, \phi = \phi w \text{ at } r = Rw$$
$$w = 0, \theta = \theta d, \phi = \phi d \text{ at } r = Rd. \quad (2)$$

Regarding third-grade liquid, the stress tensor S is described as

$$S = \eta A_1 + \alpha_1 A_2 + \alpha_2 A_1 + \tau_1 A_2 + \tau_2 (A_1 A_2 + A_2 A_1) + \tau_3 (tr A_2) A_1. \quad (3)$$

The governing parameters that apply are as follows [5–12]:

$$\nabla . w = 0, \quad (4)$$

$$\rho_f \frac{Dq}{Dt} = -\nabla p + F + J \times B, \quad (5)$$

$$(\rho c_p)_{nf} \frac{D\theta}{Dt} = k\nabla^2 \theta + \phi + (\rho c_p)_{nf} \left[D_B \nabla\theta . \nabla\phi + \left(\frac{DT}{\theta d} \right) \nabla\theta . \nabla\theta \right], \quad (6)$$

$$\frac{D\phi}{Dt} = D_b \nabla^2 \phi + \left(\frac{D_T}{\theta_d} \right) \nabla^2 \theta. \quad (7)$$

The parameters involve in the exceeding balances are well-defined in the nomenclature given at the end of the article.

The electrical field is presented in a positive radially normal direction towards the wire, and the resultant magnetic force is believed to be insignificant. As a result, effective body force is determined by

$$J \times B = (0, 0, -\sigma B_0^2 w). \quad (8)$$

The dissipation factor with tensor components are as regards:

$$S_{rz} = \mu \frac{dw}{dr} + 2(\beta_2 + \beta_3) \left(\frac{dw}{dr} \right)^3, \quad (9)$$

$$S_{rr} = (\alpha_2 + 2\alpha_1) \left(\frac{dw}{dr} \right)^2, \quad (10)$$

$$S_{zz} = \alpha_2 \left(\frac{dw}{dr} \right)^2, \quad (11)$$

$$\phi = \mu \left(\frac{dw}{dr} \right)^2 + 2(\beta_2 + \beta_3) \left(\frac{dw}{dr} \right)^4. \quad (12)$$

In light of the foregoing relationships, the equation of motion (5) yields

$$2(\beta_2 + \beta_3) \frac{d}{dr} \left(r \left(\frac{dw}{dr} \right)^3 \right) + \frac{\eta}{r} \frac{d}{dr} \left(r \frac{dw}{dr} \right) - \sigma B_0^2 u = \frac{dp}{dz}, \quad (13)$$

$$-2(\alpha_2 + \alpha_3) \frac{\eta}{r} \frac{d}{dr} \left(r \frac{dw}{dr} \right) = \frac{dp}{dr}. \quad (14)$$

The flow is caused by the pressure difference, as shown by expression (13). Because there is just pull of a wire after it leaves the die, the pressure difference in the axially is insignificant. As a result, the expression (13) can be reduced to

$$2(\beta_2 + \beta_3) \frac{d}{dr} \left(r \left(\frac{dw}{dr} \right)^3 \right) + \frac{\eta}{r} \frac{d}{dr} \left(r \frac{dw}{dr} \right) - \sigma B_0^2 u = 0. \quad (15)$$

In view of equation (10), the energy equation (7) becomes

$$k\left(\frac{d^2\theta}{dr^2}+\frac{1}{r}\frac{d\theta}{dr}\right)+\mu\left(\frac{dw}{dr}\right)^2+2(\beta_2+\beta_3)\left(\frac{dw}{dr}\right)^4+(\rho c_p)_f\left(D_B\frac{d\theta}{dr}\frac{d\phi}{dr}+\frac{D_T}{\theta_d}\left(\frac{d\theta}{dr}\right)^2\right)=0, \tag{16}$$

$$D_B\left(\frac{d^2}{dr^2}+\frac{1}{r}\frac{d}{dr}\right)\phi+\frac{D_T}{\theta_d}\left(\frac{d^2\theta}{dr^2}+\frac{1}{r}\frac{d\theta}{dr}\right)=0. \tag{17}$$

The shear stress on the wire surface is calculated as follows:

$$S_{rz}|_{r=R_w}=\mu\frac{dw}{dr}+2(\beta_2+\beta_3)\left(\frac{dw}{dr}\right)^3\Bigg|_{r=R_w}. \tag{18}$$

The force acting on the die total wire exterior is as described in the following:

$$F_w=2\pi R_w L S_{rz}|_{r=R_w}. \tag{19}$$

Furthermore, the Nusselt number N_w has the following definition:

$$N_{w_r}=\frac{rqw}{K(\theta_d-\theta_w)}, \tag{20}$$

where $q_d=-k(d\theta/dr)|_{r=R_w}$ is the heat flow at the wire's surface. We propose to explore temperature dependent viscosity in this work, as previously stated. As a result, the two additional cases are investigated.

2.1. Case 1: Reynolds Model. Nondimensional viscosity is incorporated in the study as follows [12]:

$$\eta=\exp(-\beta\Omega\theta)\approx 1-\beta\Omega\theta, \tag{21}$$

where Ω is the Reynolds model parameter.

In light of (21, 22), the expressions (15)–(20) should be read as follows (without the asterisks):

$$r^*=\frac{r}{R_w},\ w^*=\frac{w}{U_w},\ \beta_0=\beta_2+\beta_3,\ \frac{R_d}{R_w}=\delta>1,\ \beta^*=\frac{\beta_0^*}{\eta\left(R_w^2\mu_0/U_w^2\right)},\ M=\frac{\sigma B_0^2R_w^2}{\mu_0},$$

$$K=\frac{R_w^2}{V_wK^*},\ \theta^*=\frac{\theta-\theta_w}{\theta_d-\theta_w},\ Br=\frac{\mu_0U_w^2}{k(\theta_d-\theta_w)},\ \mu^*=\frac{\mu}{\mu_0},\ \phi^*=\frac{\phi-\phi_w}{\phi_d-\phi_w},$$

$$Nb=\frac{D_B(\rho c_p)(\phi_d-\phi_w)}{k},\ Nt=\frac{D_T(\rho c_p)_f(\theta_d-\theta_w)}{\theta_dk}. \tag{22}$$

Dimensionless velocity and heat equations with BCs ignoring asterisks are

$$(1-\beta\Omega\theta)\left(r\frac{d^2}{dr^2}+\frac{d}{dr}\right)w+2\beta\left(3r\frac{d^2w}{dr^2}\left(\frac{dw}{dr}\right)^2+\left(\frac{dw}{dr}\right)^3\right)-\beta\Omega r\frac{d\theta}{dr}\frac{dw}{dr}-Mwr=0, \tag{23}$$

$$\left(\frac{d^2}{dr^2}+\frac{1}{r}\frac{d}{dr}\right)\theta+(1-\beta\Omega\theta)Br\left(\frac{dw}{dr}\right)^2+2Br\beta\left(\frac{dw}{dr}\right)^4+Nb\frac{d\theta}{dr}\frac{d\phi}{dr}+Nt\left(\frac{d\theta}{dr}\right)^2=0,$$
$$\frac{d^2\phi}{dr^2}+\frac{1}{r}\frac{d\phi}{dr}+\frac{Nt}{Nb}\left(\frac{d^2}{dr^2}+\frac{1}{r}\frac{d}{dr}\right)\theta=0',$$
$$w(1)=1,\theta(1)=0,\phi(1)=0,w(\delta)=0,\theta(\delta)=1,\phi(\delta)=1. \tag{24}$$

$$S_{rz}|_{r=R_w}=\mu\frac{S_{rz}Uw}{\mu_0Rw}\Bigg|_{r=1}=\left[(1-\beta\Omega\theta)\frac{dw}{dr}+2(\beta)\left(\frac{dw}{dr}\right)^3\right]\Bigg|_{r=1}, \tag{25}$$

$$F_w=\frac{Fw}{2\pi RwL}\Bigg|_{r=1}=\left[(1-\beta\Omega\theta)\frac{dw}{dr}+2(\beta)\left(\frac{dw}{dr}\right)^3\right]\Bigg|_{r=1}, \tag{26}$$

$$Nw_r=-\frac{d\theta}{dr}\Bigg|_{r=1}, \tag{27}$$

where M, Br, β, Nb, and Nt are the magnetic factor, Brinkmannnumber, non-Newtonianffactor, Brownianmmotion factor, and thermophoresis factor, respectively. The definition of each variable or parameter is given in Table 1.

2.2. Case 2: Vogel's Model. In this case, the temperature-dependent viscosity is taken as

$$\mu=\mu_0\exp\left(\frac{H}{F+\theta}-\theta_w\right). \tag{28}$$

After using the expansion we have

$$\mu=m\left(1-\frac{H}{F^2}\theta\right), \tag{29}$$

where $m=\mu_0\exp(H/F-\theta_w)$, and H and F are the viscosity parameters associated with Vogel's model.

So the nondimensional momentum and energy equations with boundary conditions omitting asteriks are

$$m\left(1-\frac{H}{F^2}\theta\right)\left(r\frac{d^2w}{dr^2}+\frac{dw}{dr}\right)+2\beta\left(3r\frac{d^2w}{dr^2}\left(\frac{dw}{dr}\right)^2+\left(\frac{dw}{dr}\right)^3\right)-\left(\frac{\mu H}{F^2}\right)r\frac{d\theta}{dr}\frac{dw}{dr}-Mwr=0, \tag{30}$$

Table 1: Nomenclature.

A_1, A_2, A_3: Kinematic tensors	B0: Magnetic field strength	D_T: Thermophoretic diffusion coefficient	L_1: Velocity vector	J: Current density
B: Magnetic field	cp: Specific heat	F: Force	L: Length	k: Thermal conductivity
Br: Brinkman number	D_B: Brownian diffusion coefficient	D, B, B∗: Vogel's model viscosity parameters	r: Radial direction	w: Velocity component
M: Magnetic parameter	Nt: Thermophoresis parameter	p: Pressure	S: Stress tensor	Uw: Velocity of the wire
Nb: Brownian motion parameter	m: Reynolds model viscosity parameter	q: Velocity field;	T: Transpose of the matrix	$\alpha_1, \alpha_2, \beta_1, \beta_2, \beta_3$: Material constants
μ: Viscosity	μ_0: Reference viscosity	θ; Temperature field	ϕ: Nanoparticle volume fraction field	Φ: Dissipation function
σ: Electrical conductivity	β: non-Newtonian parameter	Ω: Vogel's based viscosity parameter	ρ: Density	z: Axial direction

$$\frac{d^2\theta}{dr^2} + \frac{1}{r}\frac{d\theta}{dr} + m\left(1 - \frac{H}{F^2}\theta\right)Br\left(\frac{dw}{dr}\right)^2 + 2Br\beta\left(\frac{dw}{dr}\right)^4 + Nb\frac{d\theta}{dr}\frac{d\phi}{dr} + Nt\left(\frac{d\theta}{dr}\right)^2 = 0, \tag{31}$$

$$\frac{d^2\phi}{dr^2} + \frac{1}{r}\frac{d\phi}{dr} + \frac{Nt}{Nb}\left(\frac{d^2}{dr^2} + \frac{1}{r}\frac{d}{dr}\right)\theta = 0, \tag{32}$$

$$w(1) = 1, \theta(1) = 0, \phi(1) = 0, w(\delta) = 0, \theta(\delta) = 1, \phi(\delta) = 1. \tag{33}$$

Also equations (26) and (27) become

$$S_{rz}|_{r=R_w} = \frac{S_{rz}Uw}{\mu_0 Rw}\bigg|_{r=1} = \left[(1 - \beta m\theta)\frac{D}{F^2}\theta\frac{dw}{dr} + 2\beta\left(\frac{dw}{dr}\right)^3\right]\bigg|_{r=1}, \tag{34}$$

$$F_w = \frac{Fw}{2\pi Rw L}\bigg|_{r=1} = \left[(1 - \beta m\theta)\frac{D}{F^2}\theta\frac{dw}{dr} + 2(\beta)\left(\frac{dw}{dr}\right)^3\right]\bigg|_{r=1}. \tag{35}$$

3. Numerical Procedure and Validations of the Method

In several physical problems, the consequent differential equations are significantly nonlinear. It is challenging for investigators and scientists in computing analytical or numerical approaches to such situations. For estimating the numerical solution of nonlinear partial and ordinary differential equations, the RK4 method is one of the most successful computational methods. For the numerical analysis, Runge-Kuta fourth order method is used built in package in MATHLAB SOFTWARE by taking step size $\Delta\eta = 0.01$. The existing work's calculation is determined by the comparison between existing and published work [28] as given in Table 2. The iteration procedure was stopped until all of the nodes in the η-direction met the convergence condition 10^{-5}. Additionally, the HAM method is also applied for confirmation of the method as given in Figures 2(a) and 2(b).

Table 2: Numerical comparison of HAM, RK4 Methods, and published work [28].

r	Bvph2	ND-solve	Published work
1.0	1	1	1
1.2	0.57352365	0.57352355	0.57352355
1.4	0.40325491	0.40325480	0.40325491
1.6	0.32109323	0.32109322	0.32109321
1.8	0.21036271	0.21036601	0.21036270
2.0	0	$0.0131*10^{-21}$	$0.0020*^{-25}$

The Runge-Kutta-Fehlberg strategy is used to solve the multidegree differential equation system specified in equations (23 and 24) and (31–33), for this purpose, following transformations are applied:

$$\varsigma_1 = w, \varsigma_2 = w', \varsigma_3 = \theta, \varsigma_4 = \theta', \varsigma_5 = \phi \text{ and } \varsigma_6 = \phi'. \tag{36}$$

As a result, we get the following.

$$\begin{aligned}
\zeta_1' &= \varsigma_2,\\
\varsigma_2' &= \frac{\left[M\varsigma_1 r + \beta\Omega r\varsigma_2\varsigma_4 + (\beta\Omega\varsigma_3 - 1)\varsigma_2 - 2\beta{\varsigma_2}^2\right]}{r\left[1 + M\left(1 + 6\beta{\varsigma_2}^3 - \beta\Omega\varsigma_3\right)\right]},\\
\varsigma_3' &= \varsigma_4,\\
\varsigma_4' &= -\left(\frac{1}{r}\varsigma_4 + Br(1 - \beta\Omega\varsigma_3){\varsigma_2}^2 + 2\beta\Omega Br{\varsigma_2}^4 + Nb\varsigma_4\varsigma_6 + Nt{\varsigma_4}^2\right),\\
\varsigma_5' &= \varsigma_6,\\
\varsigma_6' &= -\left(\frac{1}{r}\varsigma_6 + \frac{Nt}{Nb}\left(\varsigma_4' + \frac{1}{r}\varsigma_4\right)\right).
\end{aligned} \tag{37}$$

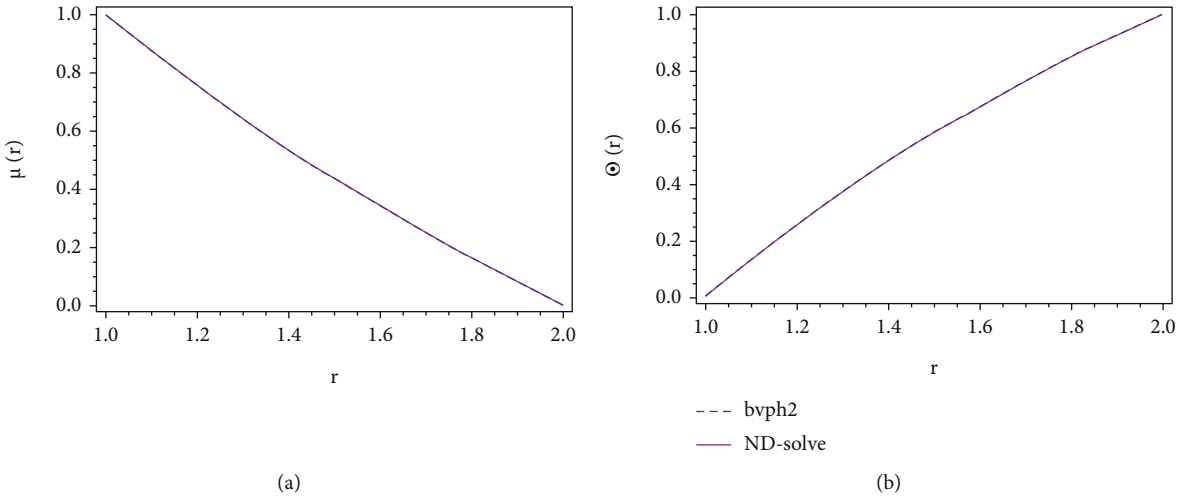

Figure 2: (a) Comparison of RK4 and HAM methods. (b) Comparison of bvph2 and ND-solve methods.

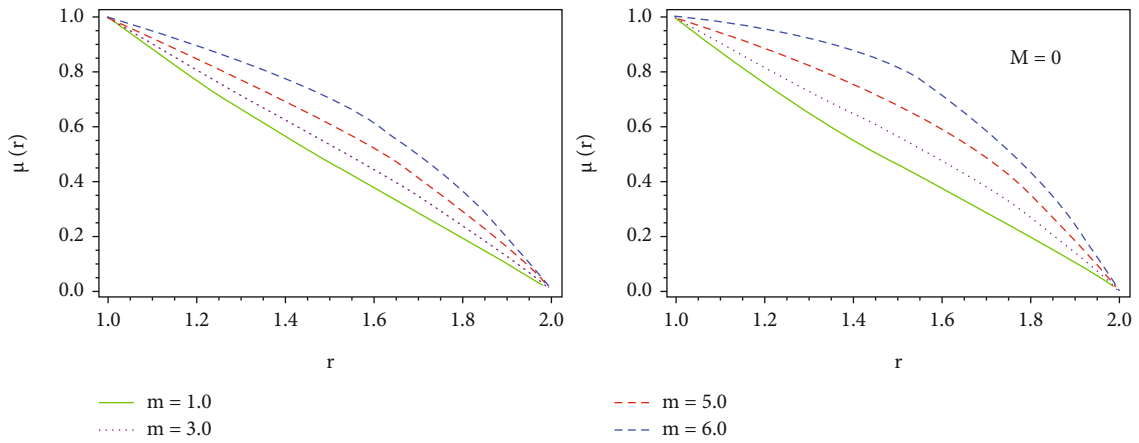

Figure 3: Consequence of m on velocity for RM.

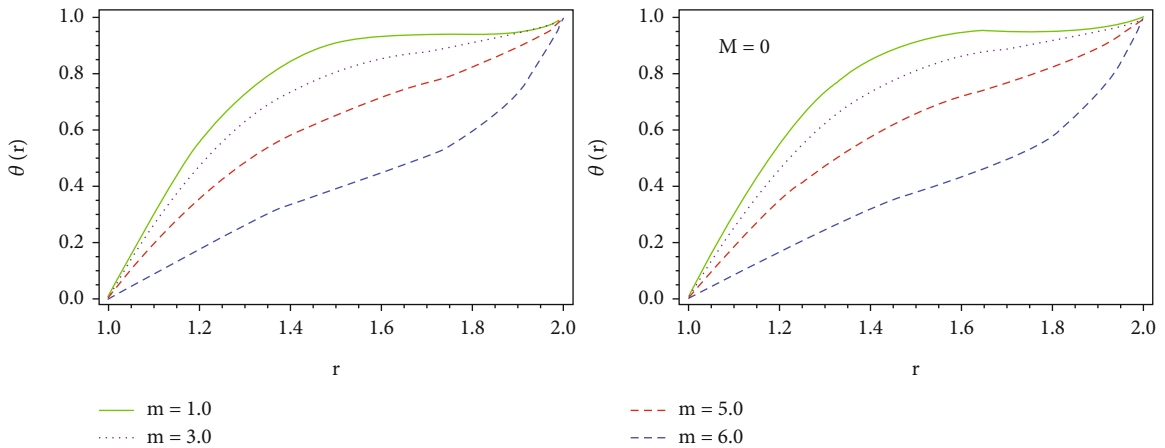

Figure 4: Consequence of m on temperature in RM.

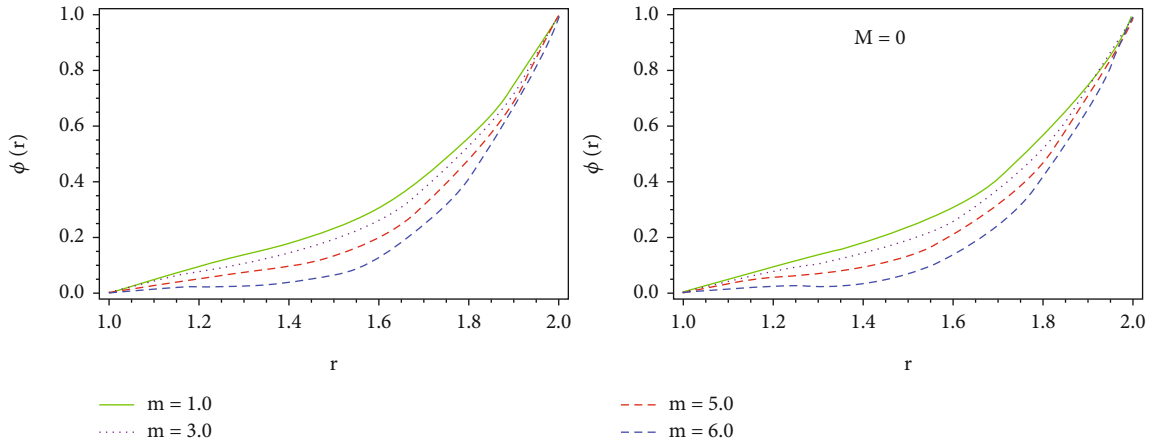

Figure 5: Consequence of m on concentration in RM.

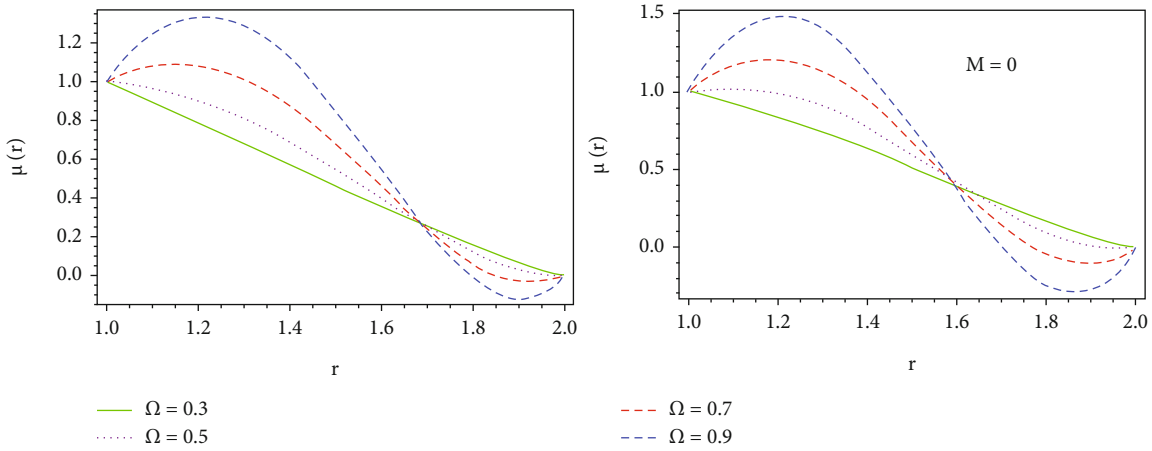

Figure 6: Consequence of Ω on velocity in VM.

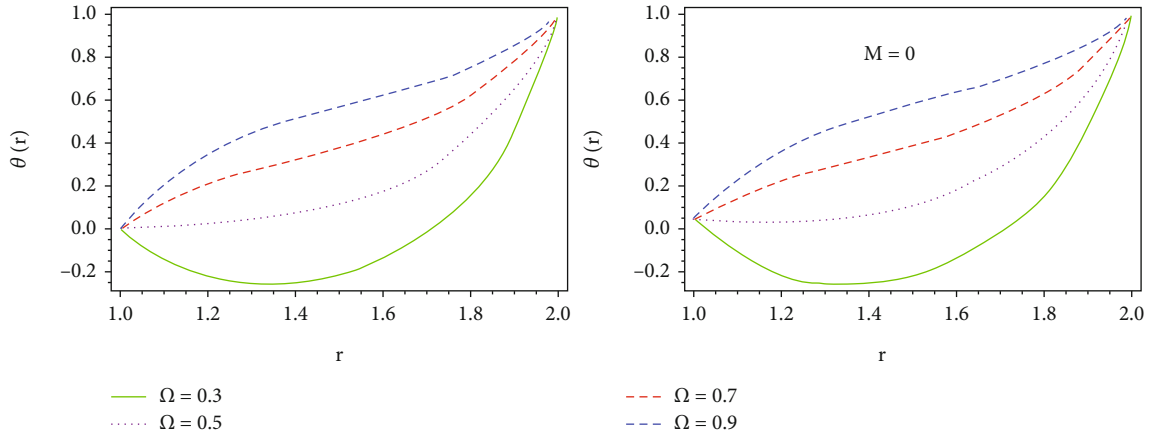

Figure 7: Consequence of Ω on temperature in VM.

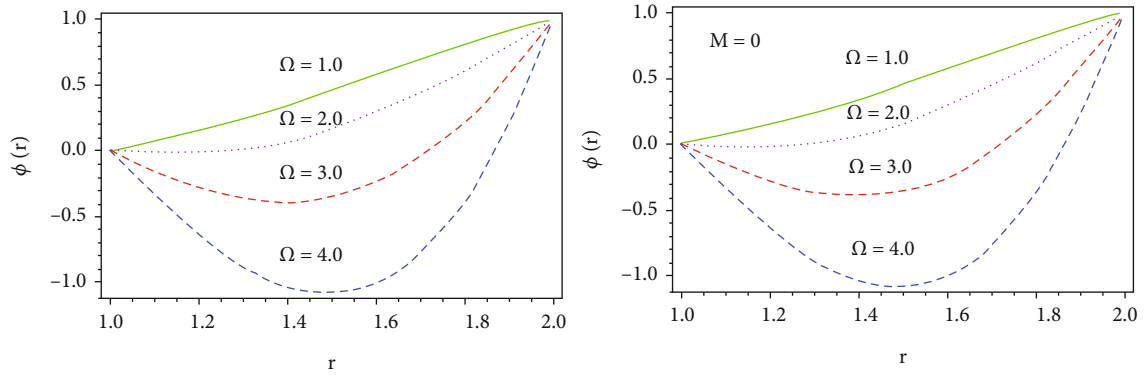

Figure 8: Consequence of Ω on concentration in VM.

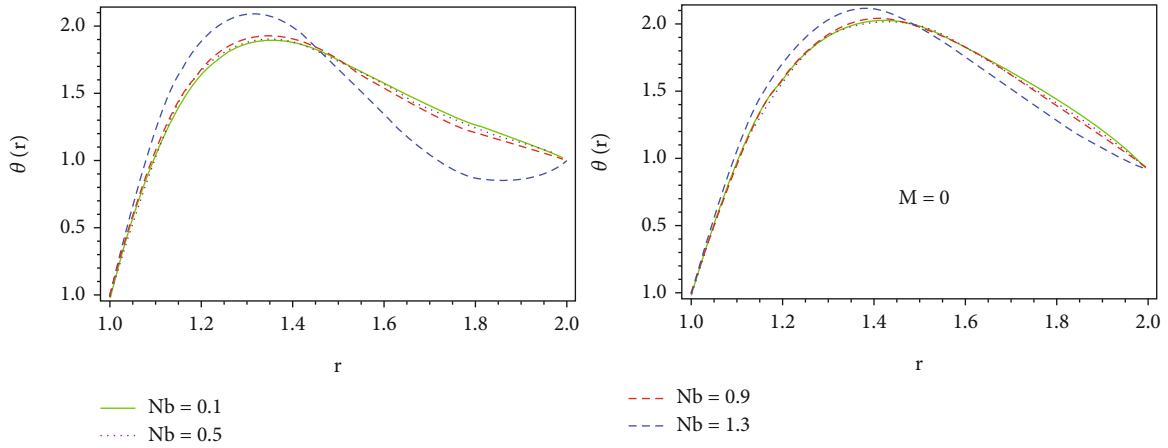

Figure 9: Consequence of *Nb* on temperature in RM.

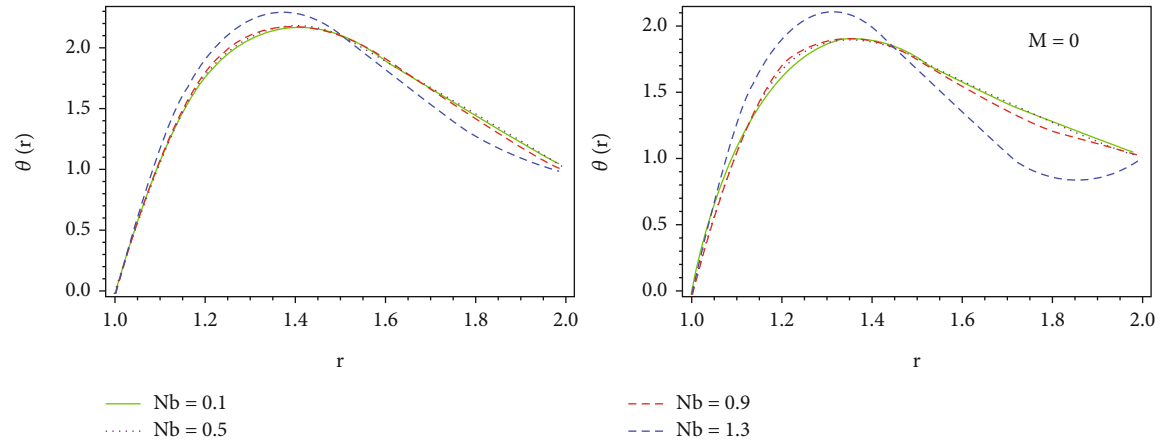

Figure 10: Consequence of *Nb* on temperature in VM.

Transferred boundary conditions are

$$\varsigma_1(1) = 1, \varsigma_2(1) = \alpha_1, \varsigma_3(1) = 0, \varsigma_4(1) = \alpha_2, \varsigma_5(1) = 0, \varsigma_6(1) = \alpha_3. \tag{38}$$

The best guess estimates for the uncertainties α_1, α_2, and α_3 are determined, and afterwards, the shooting mechanism is used to determine them.

4. Results and Discussion

For the two scenarios, RM and VM, the inspiration of essential factors on speed, heat, and nanoparticle concentration

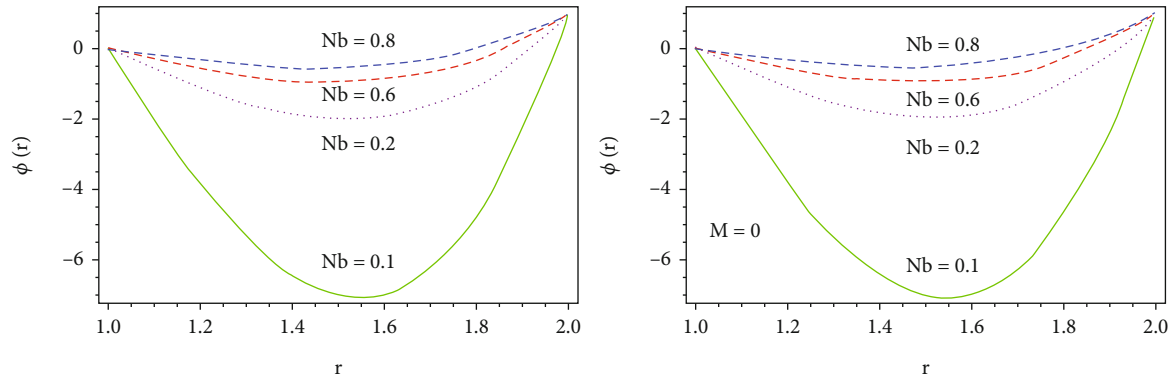

Figure 11: Consequence of Nb on concentration in RM.

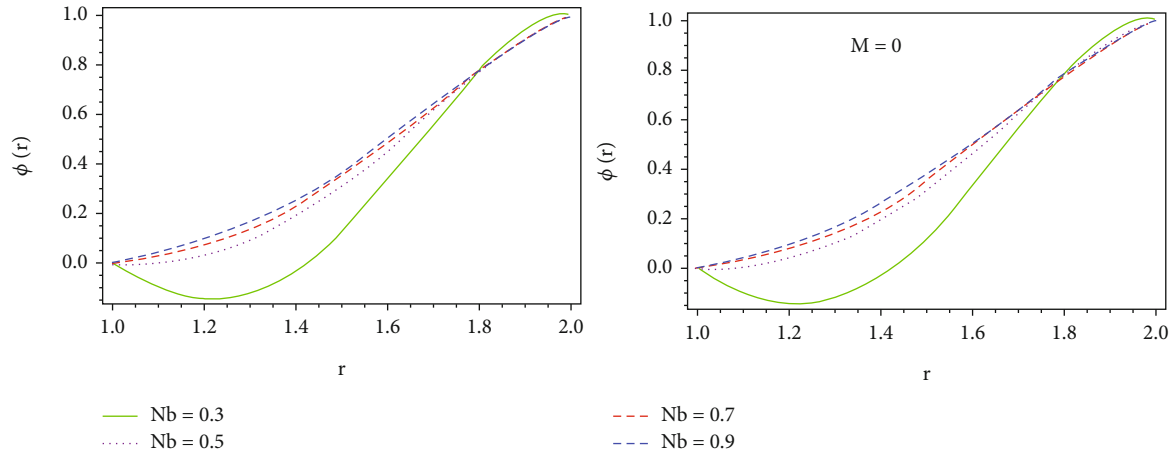

Figure 12: Consequence of Nb on concentration in VM.

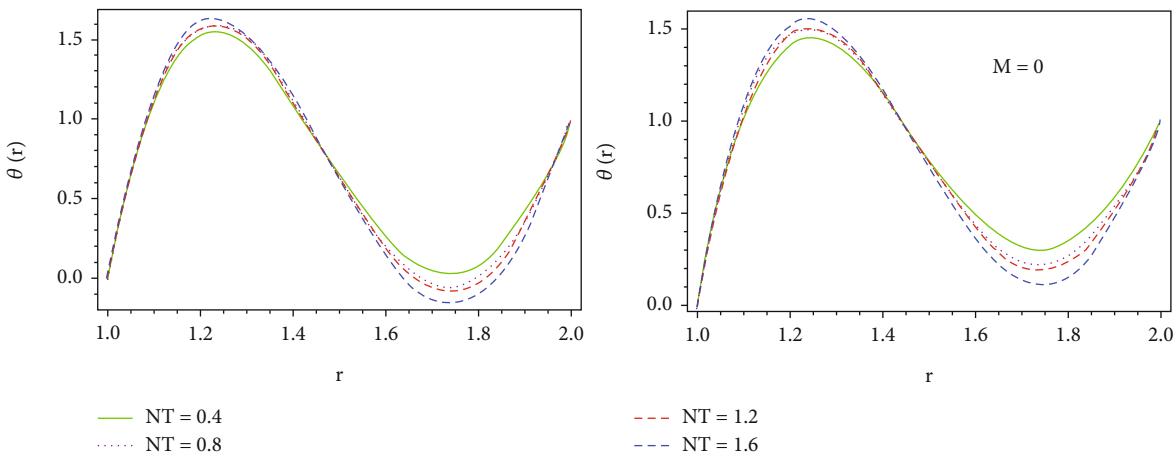

Figure 13: Consequence of Nt on temperature in RM.

outlines is explored in the occurrence and nonappearance of attractive field. The shear stress happening in the superficial of the total wire and the size of the Nusselt number on the external are estimated both for Reynolds and Vogel's model situations. The shear force happening in the surface of the total wire is proportional to $w'(r)$, as shown by equations (26), (27), (34), and (35). As a result, shear tress on a total wire surface has the same characteristic as $w'(1)$.

Figures 3–5 show the effect of m, viscosity factor on the velocity profile ($w(r)$), temperature profile ($\theta(r)$), and concentration profile ($\phi(r)$) distributions for Reynolds model, respectively. The higher values of m indicate an upsurge in

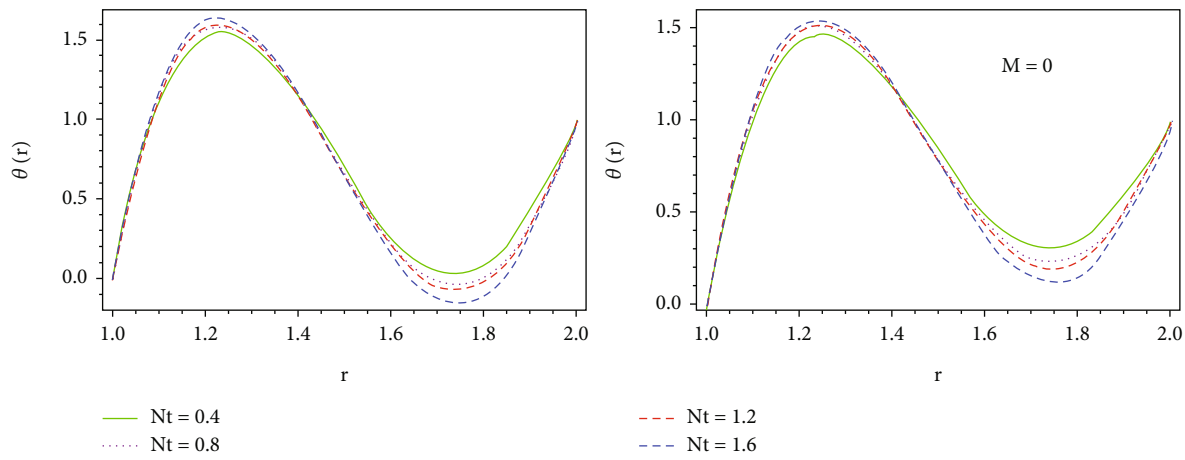

Figure 14: Consequence of Nt on temperature in VM.

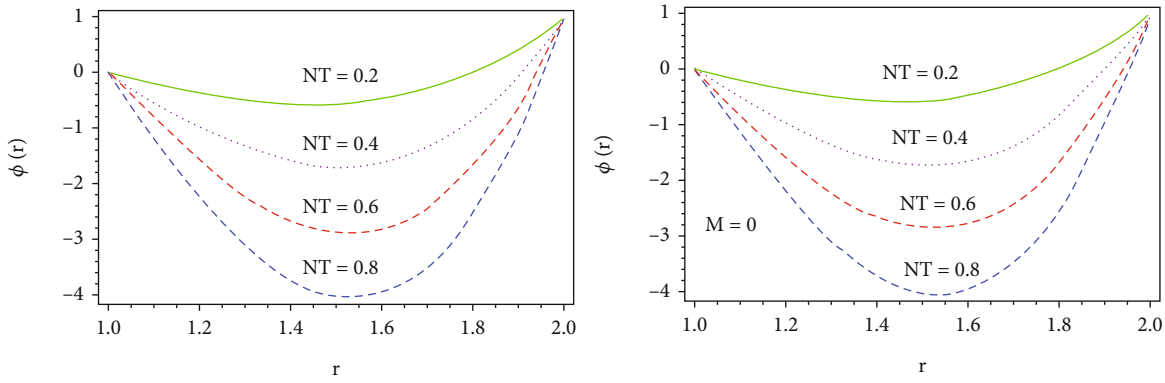

Figure 15: Consequence of Nt on concentration in RM.

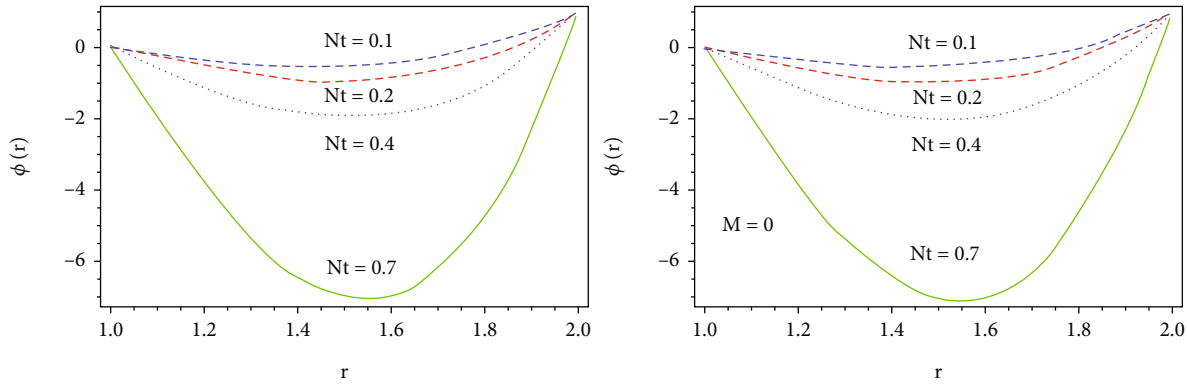

Figure 16: Consequence of Nt on concentration in VM.

velocity field but decreases in heat and concentration eprofiles. Because increasing the variable viscosity component lowers the bulk viscosity, the velocity of the fluid rises as a consequence, and the temperature and concentration profile decreases. Both the existence and absence of magnetism produce the same descriptive trend as shown in Figures 3 to 5. It is price mentioning that the in fallouts of the current study, the movement and thermal measurements match those of Shah et al. [28] study on the effect of the friction factor.

Figures 6–8 show a pictorial representation of the variances of Ω scheduled velocity, temperature, and concentration outlines. Figure 6 shows that the fluid velocity grows in the constituency $1 \leq r < 1.5$, but this behavior observed retreat in the lasting of the region. It is observed from graphs

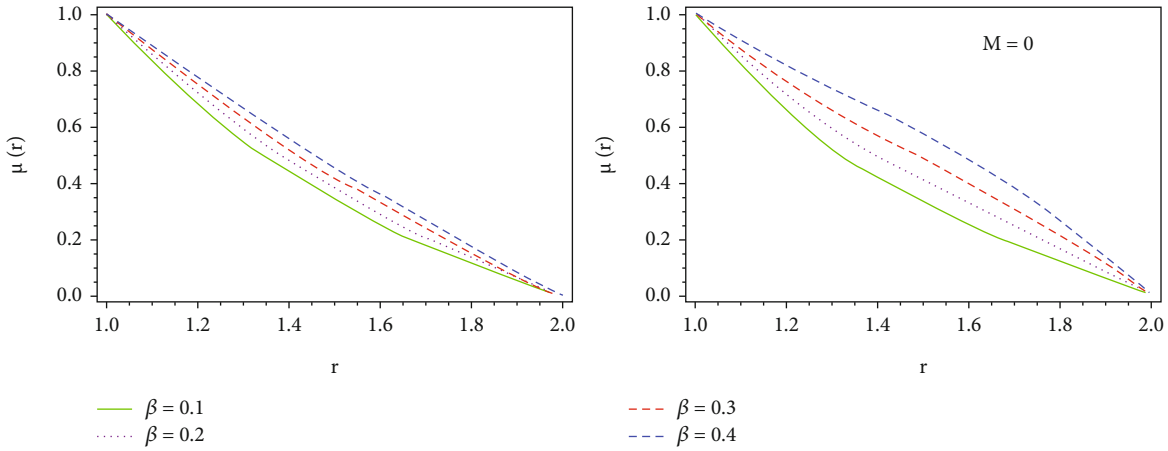

Figure 17: Consequence of Nt on velocity in RM.

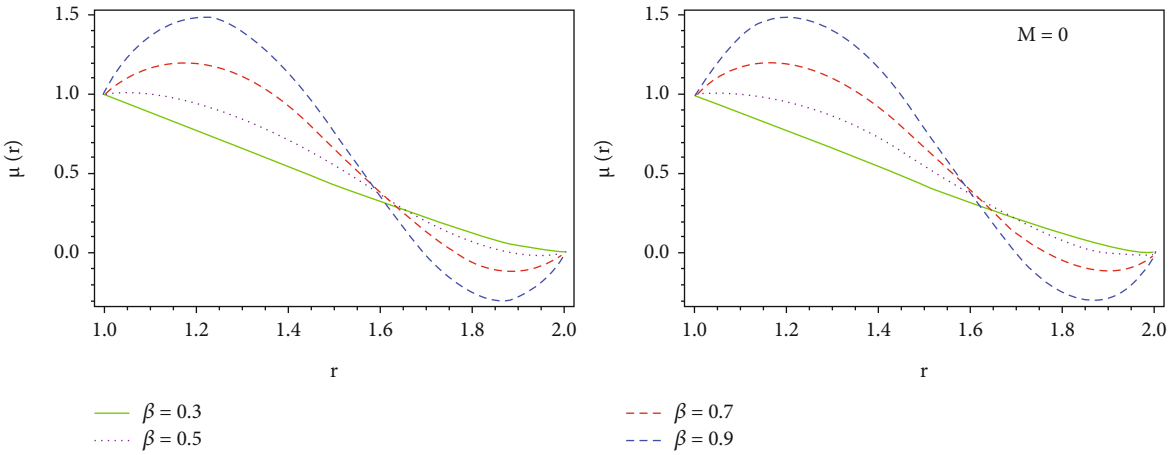

Figure 18: Consequence of β on velocity in VM.

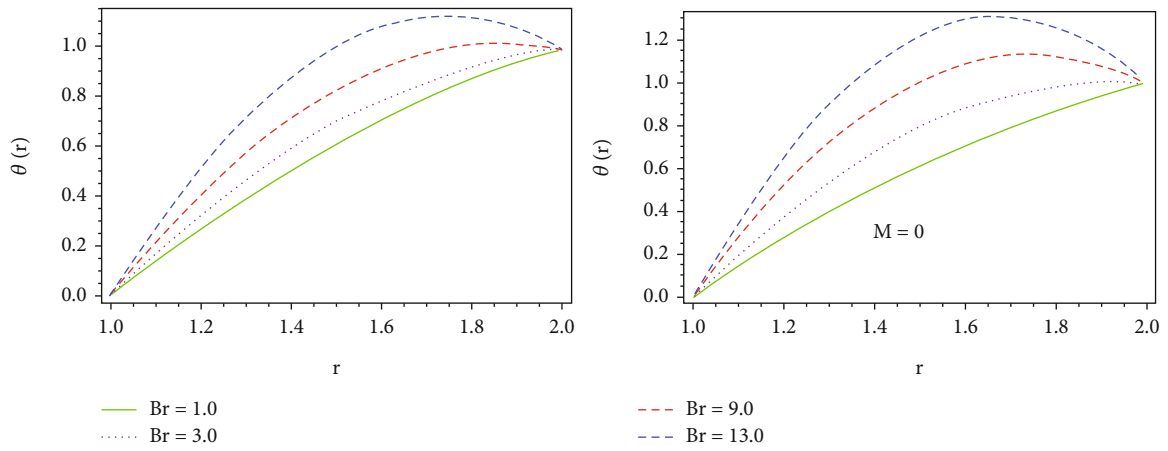

Figure 19: Consequence of Br on temperature in RM.

7 and 8 that the temperature profile increases while the concentration profiles decrease both in the presence and absence of magnetic field. Furthermore, while comparing the effects of the Reynolds model case and Vogel model case on the velocity field, we revealed that the melting velocity across the die enhances for the Reynolds model but is constrained somewhat for the Vogel model, especially near the die boundary.

Figures 9 and 10 show the variation of temperature profiles for various values of Nb. It is observed that the heat

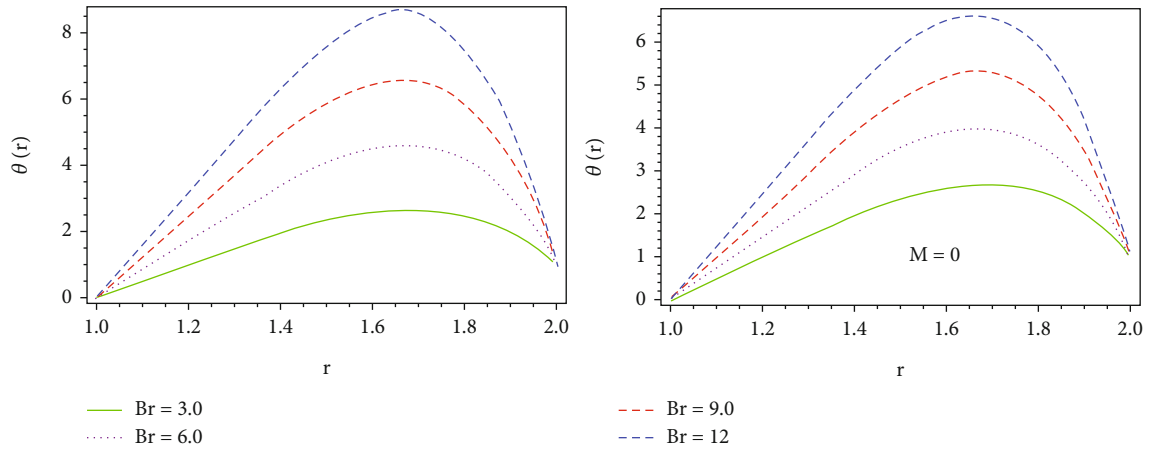

Figure 20: Consequence of Br on temperature in VM.

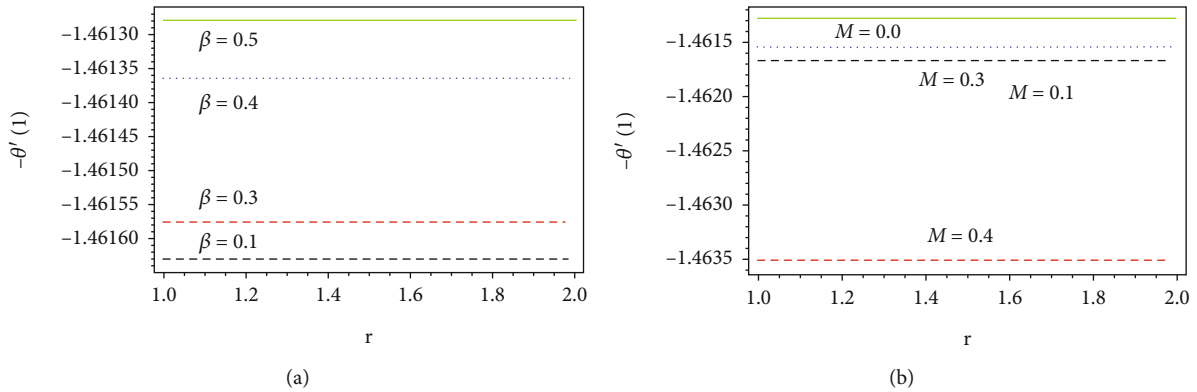

Figure 21: Impact of β and M on $-\theta'(1)$ in VM.

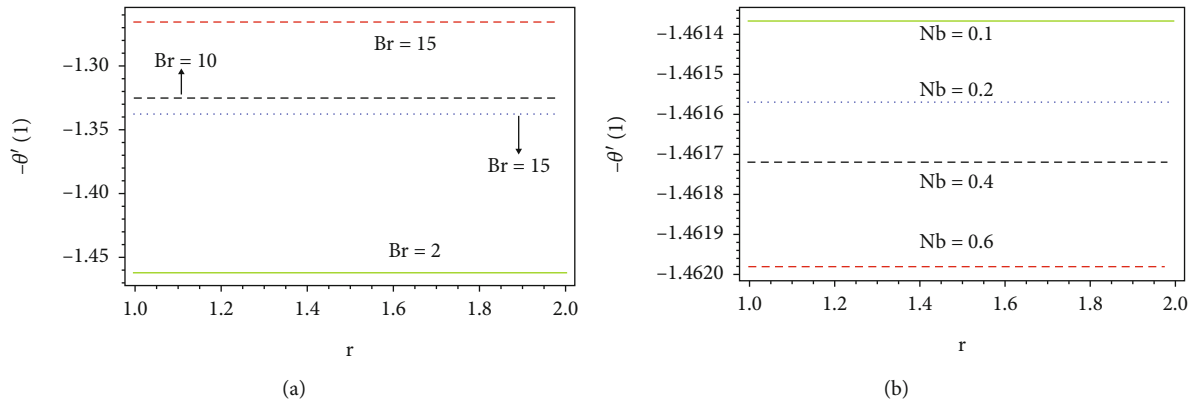

Figure 22: Impact of Br and Nb on $-\theta'(1)$ in RM.

transfer inside the die increases with the increasing vales of Nb. It is also investigated that the temperature profiles increase in the region $1 \leq r < 1.4$ for Reynolds and Vogel situations; however, the behavior in the rest of the state is the total opposite. Furthermore, in the RM situation, the temperature field, $\theta(r)$, overcomes the Vogel case. With increasing Nb, the stochastic collision among nanoparticles and liquid molecules increases, causing a flow to become heated and the nanoparticle's concentration field to decrease (see Figures 11 and 12). Furthermore, the magnetism has no discernible effect on the $\phi(r)$ field at any location on the die.

As shown in Figures 13 and 14, the significance of Nt on heat transfer rate is similar to that of Nb. The convective heat transfer force is a force that causes nanomaterials to

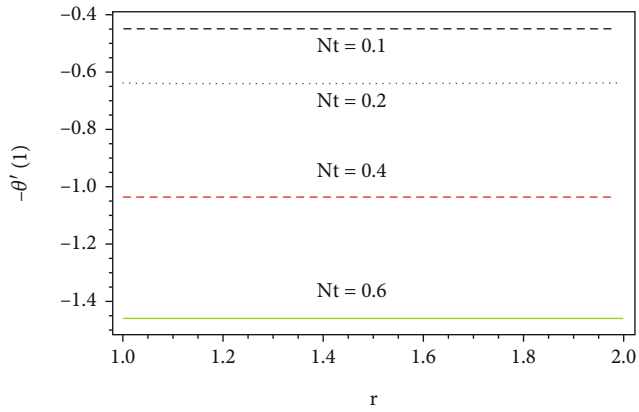

Figure 23: Impact of Nt on $\theta'(1)$ in RM case.

spread into the surrounding fluid as a conclusion of a temperature difference. The enhancement of thermophoretic force causes nanoparticles to transfer deeper into the polymer. As a result, the temperature distribution increases fashionable nearly half of a domain. Figures 15 and 16 show that the concentration profile declines as Nt increases. This is true in both cases, i.e., in the presence and absence of a magnetic field for Reynolds and Vogel models.

Figures 17 and 18 show the effect of viscoelastic parameter β on velocity profile $(w(r))$ both for Reynold and Vogel models, respectively. In non-Newtonian parameter, denominator contains rheological properties. So, the fluidity of the polymers decreases with increasing β. As a consequence, the melting polymer moment increases as the non-Newtonian parameter increases. However, the effect of β on velocity filed is additionally noticeable in the Reynolds model as compare to Vogel model. The non-Newtonian feature implies that the coating polymer movement can be increased.

The influence of Br upon $\theta(r)$ viscosity is seen in Figures 19 and 20 for the Reynolds and Vogel's model models, respectively. A larger amount of Br enhances the $\theta(r)$ profile. Brinkman number denotes the relative value of viscous heating by conduction of heat. Furthermore, in Vogel's case, the thermal profile varies substantially more for Br than in the RM case. This is validated by the results of studies published by Shah et al. [28].

Figures 21–23 show the effect of β, M, Br, Nb, and Nt on $\theta'(1)$ designed for RM and VM case. It is observed from Figures 21(a) and 21(b) that $\theta'(1)$ is larger with greater values of β and decreases in increasing M in VM case. Figures 22(a), 22(b) and 23 indicate the effect of Br, Nb, and Nt on $\theta'(1)$ for VM and RM. It is observed that $\theta'(1)$ decreases for Br, Nb, and Nt. This is true in both RM and VM scenarios. Additionally, in the situation of RM, force at the surface of the total wire plus shear and force at the surface area are greater than VM.

5. Concluded Remarks

Regarding RM and VM situations, the significance of temperature-dependent-viscosity in hydromagnetic heat/mass molecular diffusion of third-grade fluid through nanoparticle concentration is investigated. Variable viscosity has a significant impact on all fluid flow. Viscosity influences can efficiently control the heat transport of resin in a die. For bigger values of random motion and thermal radiation, the temperature gradient is enhanced in the first quarter of the section, but negative behavior occurs in the second half. Furthermore, the Brownian motion factor increases the concentration profile, but the thermophoresis factor shows a decrease. It is perceived that when the viscosity factor increases, the polymer melt flow increases, but the heat as well as concentration profile decreases. Because of increasing the variable viscosity component lowers the bulk viscosity, as a consequence, the fluid velocity rises whereas the temperature and concentration fields decrease. From this study, it is also analyzed that fluid velocity grows in the constituency $1 \le r < 1.5$, but this behavior observed retreat in the lasting. It is also investigated that the temperature profile increases while the concentration profiles decrease both in the occurrence and deficiency of magnetic field. The influence of β on velocity is additional perceptible in the Reynolds model than in the Vogel model. The non-Newtonian feature implies that the coating polymer movement can be increased. A larger amount of Br enhances the $\theta(r)$ profile since the Brinkman number denotes the relative value of viscous heating by conduction of heat. In Vogel's model, the thermoelectric field varies more strongly than in the Reynolds models case. In RM, the force happening on the total surface of wire and shear stress at the surface is greater than the VM. When RM prevails over VM, the influence of nanomaterials is positive for force on the entire wire and shear forces at the surface.

Data Availability

All relevant data are included in the manuscript. There is no data to support the present work.

Disclosure

Presentation of the manuscript as a preprint is available online from the following link https://assets.researchsquare.com/files/rs-936673/v1_covered.pdf?c=1634238080.

Conflicts of Interest

The authors declare that they have no conflicts of interest.

Authors' Contributions

Z. Khan contributed to the problem formulations and solution; I. Khan contributed to the software, coding, simulations, and wiring and manuscript communication; N. Ameer Ahammad adds an algorithm of solution or a flow chart showing which equations and in which order they are being solved, physical justification and physical meaning of the parameters, revise the model, and improved it; D. Baba Basha contributed to the results and discussion, results in computations, and conclusion; and M. Andualem

contributed to the similarity analysis of the PDEs and transformation of the PDEs into ODEs, graphs, presenting with better resolution, and improved the captions of the figures.

References

[1] K. R. Rajagopal and A. Sequira, "On the boundary conditions for fluids of the differential type," in *Navier-Stokes Equation and Related Non-Linear Problems*, pp. 273–278, Plenum press, New York, 1995.

[2] K. R. Rajagopal, P. N. Kaloni, G. A. Gram, and S. K. Malik, "Some remarks on the boundary conditions for fluids of the differential type," in *Continuum Mechanics and Its Applications, Hemisphere*, pp. 935–941, Washington DC, 1989.

[3] A. Z. Szeri and K. R. Rajagopal, "Flow of a non-Newtonian fluid between heated parallel plates," *International Journal of Non-Linear Mechanics*, vol. 20, pp. 91–101, 1985.

[4] O. D. Makinde, "Irreversibility analysis for a gravity driven non-Newtonian liquid film along an inclined isothermal plate," *PhysicaScripta*, vol. 74, no. 6, pp. 642–645, 2006.

[5] O. D. Makinde, "Thermal criticality for a reactive gravity-driven thin film flow of a third-grade fluid with adiabatic free surface down an inclined plane," *Applied Mathematics and Mechanics*, vol. 30, no. 3, pp. 373–380, 2009.

[6] M. Massoudi and I. Christie, "Effects of variable viscosity and viscous dissipation on the flow of a third grade fluid in a pipe," *International Journal of Non-Linear Mechanics*, vol. 30, no. 5, pp. 687–699, 1995.

[7] Y. Damirel and R. Kahraman, "Thermodynamic analysis of convective heat transfer in an annular packed bed," *International Journal of Heat and Fluid Flow*, vol. 21, no. 4, pp. 442–448, 2000.

[8] A. Postelnicu, T. Grosan, and I. Pop, "Free convection boundary-layer over a vertical permeable flat plate in a porous medium with internal heat generation," *International Communications in Heat and Mass Transfer*, vol. 27, no. 5, pp. 729–738, 2000.

[9] E. C. Bernhardt, *Processing of Thermoplastic Materials*, Reinhold Publishing, New York, 1962.

[10] J. M. McKelvey, *Polymer Processing*, John Wiley and Sons, New York, 1962.

[11] E. B. Bagley and S. H. Storey, "Processing of thermoplastic materials, wire wire," *Prod*, vol. 38, pp. 1104–1122, 1963.

[12] K. V. Prasad, S. R. Santhi, and P. S. Datti, "Non-newtonian power-law fluid flow and heat transfer over a non-linearly stretching surface," *Applied Mathematics*, vol. 3, no. 5, pp. 425–435, 2012.

[13] J. F. Carley, T. Endo, and W. Krantz, "Realistic analysis of flow in wire-coating dies," *Polymer Engineering and Science*, vol. 19, no. 16, pp. 1178–1187, 1979.

[14] C. D. Han, *Rheology and processing of polymeric materials volume 2 polymer processing*, vol. 2, Oxford University Press, United Kingdom, 2007.

[15] S. Middleman, *Fundamentals of Polymer Processing*, McGraw-Hill, New York, 1977.

[16] Z. Tadmor and C. G. Gogos, *Principle of Polymer Processing*, John Wiley and Sons, New York, 1978.

[17] Z. Khan, R. Shah, S. Islam et al., "MHD flow and heat transfer analysis in the wire coating process using elastic-viscous," *Coatings*, vol. 7, no. 1, p. 15, 2017.

[18] Z. Tadmor and R. B. Bird, "Rheological analysis of stabilizing forces in wire-coating dies," *Polymer Engineering and Science*, vol. 14, no. 2, pp. 124–136, 1974.

[19] B. Caswell and R. J. Tanner, "Wirecoating die design using finite element methods," *Polymer Engineering and Science*, vol. 18, no. 5, pp. 416–421, 1978.

[20] R. Wagner and E. Mitsoulis, "Effect of die design on the analysis of wire coating," *Advances in Polymer Technology*, vol. 5, Article ID 404, 325 pages, 1985.

[21] E. Mitsoulis, "Fluid flow and heat transfer in wire coating: a review," *Advances in Polymer Technology*, vol. 6, Article ID 405, 487 pages, 1986.

[22] S. Akter and M. S. J. Hashmi, "Modelling of the pressure distribution within a hydrodynamic pressure unit: effect of the change in viscosity during drawing of wire coating," *Journal of Materials Processing Technology*, vol. 77, no. 1-3, pp. 32–36, 1998.

[23] S. Akter and M. S. J. Hashmi, "Analysis of polymer flow in a conical coating unit: a power law approach," *Progress in Organic Coating*, vol. 37, no. 1-2, pp. 15–22, 1999.

[24] S. Akter and M. S. J. Hashmi, "Wire drawing and coating using a combined geometry hydrodynamic unit: theory and experiment," *Journal of Materials Processing Technology*, vol. 178, no. 1-3, pp. 98–110, 2006.

[25] C. D. Han and D. Rao, "Studies on wire coating extrusion. I. The rheology of wire coating extrusion," *Polymer Engineering and Science*, vol. 18, no. 13, pp. 1019–1029, 1978.

[26] R. Kozan and B. Cirak, "Prediction of the coating thickness of wire coating extrusion processes using artificial neural network (ANN)," *Modern Applied Science*, vol. 3, no. 7, p. 52, 2009.

[27] M. Sajid, A. M. Siddiqui, and T. Hayat, "Wire coating analysis using MHD oldroyd 8-constant fluid," *International Journal of Engineering Science*, vol. 45, no. 2-8, pp. 381–392, 2007.

[28] R. A. Shah, S. Islam, M. Ellahi, A. M. Siddhiqui, and T. Harron, "Analytical solutions for heat transfer flows of a third grade fluid in post treatment of wire coating," *International Journal of Physical Sciences*, vol. 6, pp. 4213–4223, 2011.

[29] D. M. Binding, A. R. Blythe, S. Guster, A. A. Mosquera, P. Townsend, and M. P. Wester, "Modelling polymer melt flows in wirecoating processes," *Journal Of Non-Newtonian Fluid Mechanics*, vol. 64, no. 2-3, pp. 191–206, 1996.

[30] I. Multu, I. Twnsend, and M. F. Webster, "Simulation of cable-coating viscoelastic flows with coupled and decoupled schemes," *Journal Of Non-Newtonian Fluid Mechanics*, vol. 74, no. 1-3, pp. 1–23, 1998.

[31] M. Kasajima and K. Ito, "Post-treatment of polymer extrudate in wire coating," *Applied Polymer Symposia*, vol. 20, pp. 221–235, 1973.

[32] S. Baag and S. R. Mishra, "Power law fluid model in post treatment analysis of wire coating with linearly varying temperature," *American Journal of Heat and Mass Transfer*, vol. 2, no. 2, pp. 89–107, 2015.

[33] K. Kim, H. H. Kwak, S. H. Park, and Y. S. Lee, "Theoretical prediction on double-layer coating in wet-on-wet optical fiber coating process," *Journal of Coatings Technology and Research*, vol. 8, no. 1, pp. 35–44, 2011.

[34] K. Kim and H. H. Kwak, "Analytic study of non-Newtonian double layer coating liquid flows in optical fiber manufacturing," *Trans Tech Publications*, vol. 224, pp. 260–263, 2012.

[35] R. A. Zeeshan, S. I. Shah, and A. M. Siddique, "Double-layer optical fiber coating using viscoelastic Phan-Thien-Tanner fluid," *New York Science Journal*, vol. 6, pp. 66–73, 2013.

[36] Z. Khan, S. Islam, R. A. Shah, I. Khan, and T. Gu, "Exact solution of PTT fluid in optical fiber coating analysis using two-layer coating flow," *Journal of Applied Environmental and Biological Sciences*, vol. 5, pp. 96–105, 2015.

[37] Z. Khan, S. Islam, R. A. Shah, and I. Khan, "Flow and heat transfer of two immiscible fluids in double-layer optical fiber coating," *Journal of Coating Technology and Research*, vol. 13, no. 6, pp. 1055–1063, 2016.

[38] A. Aziz, "A similarity solution for laminar thermal boundary layer over a flat plate with a convective surface boundary condition," *Communications in Nonlinear Science and Numerical Simulation*, vol. 14, no. 4, pp. 1064–1068, 2009.

[39] M. I. Khan, T. Hayat, and A. Alsaedi, "*Numerical analysis for Darcy-Forchheimer flow in presence of homogeneous-heterogeneous reactions*," *Results in Physics*, vol. 7, pp. 2644–2650, 2017.

[40] A. Shafiq, S. A. Lone, T. N. Sindhu, Q. M. Al-Mdallal, and G. Rasool, "Statistical modeling for bioconvective tangent hyperbolic nanofluid towards stretching surface with zero mass flux condition," *Scientific Reports*, vol. 11, no. 1, pp. 1–11, 2021.

[41] A. Shafiq, T. N. Sindhu, and C. M. Khalique, "Numerical investigation and sensitivity analysis on bioconvective tangent hyperbolic nanofluid flow towards stretching surface by response surface methodology," *Alexandria Engineering Journal*, vol. 59, no. 6, pp. 4533–4548, 2020.

[42] T. Hayat, A. Shafiq, A. Alsaedi, and S. Asghar, "Effect of inclined magnetic field in flow of third grade fluid with variable thermal conductivity," *AIP Advances*, vol. 5, no. 8, article 087108, 2015.

[43] T. Hayat, A. Shafiq, and A. Alsaedi, "Effect of Joule heating and thermal radiation in flow of third grade fluid over radiative surface," *PLoS One*, vol. 9, no. 1, article e83153, 2014.

[44] T. N. Sindhu and A. Atangana, "Reliability analysis incorporating exponentiated inverse Weibull distribution and inverse power law," *Quality and Reliability Engineering International.*, vol. 37, no. 6, pp. 2399–2422, 2021.

[45] A. Naseem, A. Shafiq, L. Zhao, and M. U. Farooq, "Analytical investigation of third grade nanofluidic flow over a Riga plate using Cattaneo-Christov model," *Results in Physics*, vol. 9, pp. 961–969, 2018.

[46] A. Shafiq, F. Mebarek-Oudina, T. N. Sindhu, and A. Abidi, "A study of dual stratification on stagnation point Walters' B nanofluid flow via radiative Riga plate: a statistical approach," *The European Physical Journal Plus*, vol. 136, no. 4, pp. 1–24, 2021.

[47] T. Hayat, A. Shafiq, A. Alsaedi, and M. Awais, "MHD axisymmetric flow of third grade fluid between stretching sheets with heat transfer," *Computers & Fluids*, vol. 86, pp. 103–108, 2013.

[48] A. Shafiq, A. B. Çolak, and T. N. Sindhu, "Designing artificial neural network of nanoparticle diameter and solid–fluid interfacial layer on single-walled carbon nanotubes/ethylene glycol nanofluid flow on thin slendering needles," *International Journal for Numerical Methods in Fluids.*, vol. 93, no. 12, pp. 3384–3404, 2021.

[49] M. Sheikholeslami, T. Hayat, and A. Alsaedi, "RETRACTED: Numerical simulation of nanofluid forced convection heat transfer improvement in existence of magnetic field using lattice Boltzmann method," *International Journal of Heat and Mass Transfer*, vol. 108, pp. 1870–1883, 2017.

[50] T. Hayat, M. I. Khan, M. Waqas, A. Alsaedi, and M. Farooq, "Numerical simulation for melting heat transfer and radiation effects in stagnation point flow of carbon-water nanofluid," *Computer Methods in Applied Mechanics and Engineering*, vol. 315, pp. 1011–1024, 2017.

[51] M. Waqas, M. I. Khan, T. Hayat, and A. Alsaedi, "Numerical simulation for magneto Carreau nanofluid model with thermal radiation: a revised model," *Computer Methods in Applied Mechanics and Engineering*, vol. 324, pp. 640–653, 2017.

[52] B. Mahanthesh, B. J. Gireesha, R. R. Gorla, F. M. Abbasi, and S. A. Shehzad, "Numerical solutions for magnetohydrodynamic flow of nanofluid over a bidirectional non-linear stretching surface with prescribed surface heat flux boundary," *Journal of Magnetism and Magnetic Materials*, vol. 417, pp. 189–196, 2016.

[53] Z. Khan and I. Khan, "Temperature-dependent viscosity and nanoparticle effect on wire coating using third-grade as a polymer liquid with magnetic field flow within porous die, preprint," 2021.